

GALAXY-QUASAR CORRELATIONS BETWEEN APM GALAXIES AND HAMBURG-ESO QSOS

Joshua G. Nollenberg¹, Liliya L.R. Williams

Astronomy Department, School of Physics and Astronomy, University of Minnesota, 116 Church St. S.E., Minneapolis, MN 55455

jgnollenberg@stthomas.edu, llrw@astro.umn.edu

ABSTRACT

We detect angular galaxy-QSO cross-correlations between the APM Galaxy Catalogue and a preliminary release (consisting of roughly half of the anticipated final catalogue) of the Hamburg-ESO Catalogue of Bright QSOs as a function of source QSO redshift using multiple cross-correlation estimators. Each of the estimators yield very similar results, implying that the APM catalogue and the Hamburg-ESO survey are both fair samples of the respective true galaxy and QSO populations. Though the signal matches the expectations of gravitational lensing qualitatively, the strength of the measured cross-correlation signal is significantly greater than the CDM models of lensing by large scale structure would suggest. This same disagreement between models and observation has been found in several earlier studies. We estimate our confidence in the correlation detections versus redshift by generating 1000 random realizations of the Hamburg-ESO QSO survey: We detect physical associations between galaxies and low-redshift QSOs at 99% confidence and detect lensing associations at roughly 95% confidence for QSOs with redshifts between 0.6 and 1. Control cross-correlations between Galactic stars and QSOs show no signal. Finally, the overdensities (underdensities) of galaxies near QSO positions relative to those lying roughly 135–150' away are uncorrelated with differences in Galactic extinction between the two regions, implying that Galactic dust is not significantly affecting the QSO sample.

Subject headings: gravitational lensing: galaxies: catalogs: large scale structure of the Universe

¹Current address: Department of Physics, University of St. Thomas, OWS 153, 2115 Summit Ave., St. Paul, MN 55105

1. Introduction

Turner (1980), noting the ‘apparent extreme evolution’ of the QSO luminosity function, first indicated along with Canizares (1981) that magnification bias due to gravitational lensing could create statistical associations between foreground galaxies and high-redshift QSOs. A number of studies have since examined the phenomenon.

Magnification bias arises when foreground gravitational lenses (i.e. galaxy clusters or large scale structure) magnify the source planes of background objects (QSOs). This source plane magnification results in two effects: 1) Individual sources span a larger area on the sky than they would if a lens were not present. Because gravitational lensing conserves flux, this results in a net brightening of the source, which can lead to the inclusion of otherwise undetectable objects in a flux-limited sample. 2) The number density of the sources on the sky is decreased because of the same stretching of the source plane by the lens.

Assuming a flux-limited sample of QSOs, depending on the slope of the magnitude number counts of a sample of selected sources, α_m , the combination of the two effects produces a statistical association, $\omega_{GQ}(\theta)$, or alternatively an overdensity (or underdensity), $q(\theta)$, which is dependent on the magnification, $\mu(\theta)$:

$$q(\theta) - 1 = \omega_{GQ}(\theta) = \mu(\theta)^{2.5 \cdot \alpha_m - 1} - 1. \quad (1)$$

If $\alpha_m > 0.4$, positive correlations will be observed, whereas negative correlations will occur if $\alpha_m < 0.4$. Should α_m equal the critical value of 0.4, no correlations will be detected regardless of lens magnification. Finally, the amount of magnification depends on the projected surface mass density of the lens and on the relative distances of sources and lenses from the observer.

There are, however, complications. For instance, if dust were located inside galaxy clusters, then QSOs lying on lines of sight near foreground clusters would tend to be more heavily obscured than those not lying behind clusters. This would result in a net decrease in a measured galaxy-QSO cross-correlation. A wide variety of techniques have been used to search for dust in galaxy clusters spanning their range in cluster richness. For a more complete description of past work in this area, please refer to the introduction section of Nollenberg et al. (2003). Early studies performed on the basis of visual inspection (Zwicky 1962; Karachentsev & Lipovetskii 1969; de Vaucouleur, de Vaucouleur & Corwin 1972) tended to report rather large amounts of extinction (up to $A_V \sim 0.4$ magnitudes) in clusters such as Coma and Virgo. Smaller (though occasionally mutually inconsistent) estimates have been reported by later studies (Wise et al. 1993; Hu 1992; Bahcall 1999; Arnaud & Mushotzky 1998; Voit & Donahue 1995; Annis & Jewitt 1993; Romani & Maoz 1992; Véron-Cetty & Véron 1989; Maoz 1995; Dwek, Rephaeli & Mather 1990; Ferguson 1993; Biviano et al. 1990; Nollenberg et al. 2003), including upper limits of $E(B - V) \approx 0^m02$

and $A_R = 0^m025$ on reddening and extinction by large scale distributions of dust within medium-richness APM clusters, respectively (Nollenberg et al. 2003). Low levels of dust in galaxy clusters such as this imply that cluster dust does not significantly contribute to galaxy-QSO associations, though the matter has not yet been entirely resolved because the possibility exists that dust may reside in small clumps which could have escaped detection using the Nollenberg et al. (2003) technique.

Galactic dust is also a thorny issue because its presence could result in positive correlations between galaxies and QSOs or between galaxy clusters and QSOs. Due to the fact that Galactic dust extinguishes light from galaxies and QSOs alike, the observer would tend to see QSOs and galaxies that lie in the same unobscured parts of the sky, yielding a positive statistical association. Its distribution is also quite filamentary and this structure continues to scales smaller than are sampled by either the $\sim 6'.1$ pixel size of the Schlegel, Finkbeiner & Davis (1998) extinction map or the lower resolution Burstein & Heiles (1982) map. High-contrast filaments of dust could therefore obscure individual sources, and while statistical association measurements generally sample scales much larger than this, Galactic dust could in principle leave its imprint by introducing power on a wide variety of scales that are dependent on the topology of the dust distribution itself.

This paper is organized as follows: After a discussion of prior results in Section 2, we will describe the galaxy and QSO data that we use in Section 3. Then we will discuss our methods for estimating galaxy-QSO cross-correlations in Section 4. Following this, we will discuss the results of our analysis, including measurements of angular cross-correlations, integrated cross-correlations vs. redshift, confidence tests and comparisons with models through the remainder of Section 4. Finally, we summarize our results in Section 5.

2. Earlier Studies

Many past observations qualitatively support the statistical lensing picture. Characteristics of their respective studies, including galaxy and QSO catalogues, brightness ranges, QSO redshift ranges, as well as the observed association, can be found in Table 1. The ‘Detected’ column indicates the type of statistically significant cross-correlations that were detected. ‘+’, ‘0’ and ‘–’ refer to *positive*-, *no*-, and *negative*-correlations, respectively. The studies are divided into three groups from the top of the table to bottom, respectively: *Top*: Measurements of galaxy overdensities using incomplete QSO samples. *Middle*: Galaxy-QSO angular cross-correlations using complete sets of optically-selected (or in one case, UV-selected) QSOs. *Bottom*: Cross-correlations involving complete catalogues of radio-selected QSOs. *Note*: Romani & Maoz (1992) and Maoz (1995) are also mentioned in the introduc-

tory text, though they did not specifically measure overdensities or cross-correlations using a single range of QSO magnitudes and are as a result not listed on this table.

Several early studies, including those found in the top portion of Table 1: Tyson (1986); Fugmann (1988, 1990); Hammer & Le Fèvre (1990); Hintzen et al. (1991); Bartelmann & Schneider (1994), and Drinkwater et al. (1992); were conducted using heterogeneous or incomplete QSO samples, often involving portions of the Hewitt & Burbidge (1980) or Véron-Cetty & Véron (1989) QSO catalogues, and searched for associations of foreground galaxies within some angular scale around background QSOs relative to the field average. Not all of these studies necessarily attributed measured overdensities with gravitational lensing. However, even those studies that did not attribute them to lensing do, in retrospect, qualitatively agree with the magnification bias picture.

While using optically-selected QSO catalogues, at least four studies found positive correlations, as expected on the basis of their specific QSO magnitude cuts. Webster et al. (1988) detected positive correlations between QSOs and galaxies on arcsecond scales and indicated that the foreground lensing mass must be much greater than that associated with the visible galaxies themselves. Rodrigues-Williams & Hogan (1994) observed an overdensity of LBQS QSOs with $1.4 < z < 2.2$ and $B \leq 18^m5$ within $6.6h^{-1}$ Mpc of Zwicky clusters (which have a typical redshift around 0.2) with 4.7σ significance. Another study, by Williams & Irwin (1998) explored statistical correlations between LBQS QSOs and APM galaxies with a median redshift of $z \approx 0.25$. Significant positive correlations were found on angular scales $< 100'$, using a sample of QSOs at redshifts $z > 1$ with magnitudes $B_J \leq 18^m0$. Finally, Gaztañaga (2003) used Sloan Digital Sky Survey Early Data Release galaxies and QSOs (albeit a heterogenous sample) and found cross-correlations on scales $< 10'$. Each of these studies measured cross-correlations that were a few times larger than what would be expected from CDM large scale structure lensing models.

Even though the amplitudes of correlations are typically much greater than expected from models, the signal is most probably due to lensing because of the unique signature of lensing: Positive, negative and null correlations have been detected using QSO samples with the expected corresponding brightness cuts. This may hold true for some studies that were not originally looking into gravitational lensing as well. Boyle, Fong & Shanks (1988), for example, detected a 30% deficiency in the number of $B < 20^m0$ high-redshift UVX-selected QSOs at separations within $4'$ of foreground clusters of galaxies. Citing extinction due to dust as the simplest explanation, they ascribed an average extinction of $A_V \approx 0^m2$ to their set of clusters. However, an anti-correlation is expected within the magnification bias picture for QSOs with this limiting magnitude due to the resulting shallow slope, α_m . In fact, Croom & Shanks (1999) investigated the Boyle, Fong & Shanks (1988) anti-correlation under the

assumption that statistical lensing was the cause and found no discrepancy in interpretation between it and the positive correlation measured by Williams & Irwin (1998). Similarly, Romani & Maoz (1992) measured a $\sim 25\%$ dearth of high-redshift QSOs within $60'$ of nearby Abell Clusters and explained that it could be accounted for by the presence of $A_B = 0^m15$ of extinction within the clusters. Later analysis by Maoz (1995) tested the presence of dust by looking for differences between the colors of QSOs that lay within 1° of Abell clusters with those outside of that separation. No difference was found and tight constraints on reddening were given: $E(B-V) \leq 0^m06$ to 90% confidence. Just as in the case of Boyle, Fong & Shanks (1988), the anti-correlations that were measured in the Romani & Maoz (1992) work can likely be explained in terms of magnification bias. Romani & Maoz (1992) show that the average QSO magnitude in their sample increases with decreasing QSO-cluster separation. In fact, the average magnitude reaches $V \sim 19$ for separations within $10'$. Because the *limiting* magnitude is important in magnification bias, while neither individual QSO magnitudes nor limiting magnitudes of the QSO sample are given, it is quite likely that the slope, α_m decreases with decreasing separation (and increasing limiting magnitude, inferred from the increase in the average magnitude). This would render a result consistent with weak lensing.

A natural way to test for the influence of dust (Galactic or extragalactic) would be to compare cross-correlations involving optically-selected QSOs with those that utilize radio-selected ones. Many of the older studies listed above do use radio-selected QSOs. In addition, several studies have incorporated radio-selected QSOs in order to determine whether extinction is important. Comparing radio- and optically-selected subsets of QSOs from the Parkes and LBQS catalogues, respectively, with similar redshift distributions ($z \geq 0.3$), Benítez & Martínez-González (1997) noted a $\approx 99\%$ significant excess of radio QSOs within $10'$ of COSMOS/UKST galaxies. The Parks excess is anti-correlated with the LBQS ($B_J < 20^m5$) sample at high confidence. And while magnification bias can account for part of the difference, they argue that dust could account for the rest if the extinction were present in clusters at a level consistent with Maoz (1995). Norman & Williams (2000) measured correlations between 1 Jy QSOs and APM galaxies on degree scales and found positive correlations that are inconsistent with a Galactic dust scenario while Benítez et al. (2001) used two complete samples of QSOs and found a similar result with the added caveat that the introduction of strong lensing could help to describe the discrepancy between lensing observations and models on smaller angular scales.

In general, prior work in galaxy-QSO associations are at least qualitatively consistent with expectations from magnification bias, though some measurements yielded results that were significantly greater than predicted by CDM large scale structure lensing models. However, inspection of Table 1 demonstrates that those studies using faint optical QSOs tend to have negative correlations while those that used bright QSOs found positive correlations.

This is entirely consistent with Equation 1.

3. Data

3.1. APM Catalogue

Our galaxy data originated from the UKST SES B_J and R sky surveys, the photometry of which have been digitized using the Automated Plate Machine (APM) at the University of Cambridge (Irwin 1996). The APM galaxy catalogue, which has limiting magnitudes of $B_J \approx 22.5$ and $R \approx 21$, is complete to magnitudes of $B_J \approx 20.5$ and $R \approx 19.5$ with some plate-to-plate variation due to uncertainties in absolute photometric calibration and variations in sky background for each field. We have not sought to correct for the variation in photometric calibration, rather we adopt an analysis strategy that should remove its effect, as we will describe in Section 4.1. We culled objects that were detected and classified as galaxies in the R band with magnitudes in the range $18.5 \leq R \leq 20$ from 209 $5^{\circ}8' \times 5^{\circ}8'$ UKST sky survey fields lying at declinations below $+2.5^{\circ}$.

Because the catalogue is derived from a photographic Schmidt survey, vignetting is a factor on individual UKST plate fields. It reduces the plate density of objects, but the magnitude of the effect is negligible within a radius of $2^{\circ}7'$ from respective UKST field centers. Hence in order to avoid the contamination of the galaxy-QSO cross-correlation, we remove all galaxies lying more than $2^{\circ}7'$ from their respective field centers from our study. The locations of the galaxies used in our study, along with QSO positions can be found in Figure 1.

We estimated the redshift distribution of galaxies in our magnitude cut using the fit given by Baugh & Efstathiou (1993). The parameters of this fit match the observed magnitude-binned galaxy redshift distributions from the Stromlo/APM redshift survey (Loveday et al. 1992a,b), as well as the Durham/Anglo-Australian Telescope faint galaxy redshift survey conducted by Broadhurst, Ellis & Shanks (1988) and the LDSS faint galaxy survey by Colless et al. (1990, 1993). (Please see Section 4.1 of Maddox, Efstathiou & Sutherland (1996) for more details regarding the development of this fit.) The resulting distribution (with arbitrary normalization), shown as a solid curve in Figure 2, peaks at a redshift of $z \approx 0.25$ and falls off almost entirely by $z \sim 0.5 - 0.6$. The galaxy sample does overlap the low-redshift portion of our QSO sample (see Section 3.2), which we retain to investigate differences between the cross-correlation signals due to physical associations and magnification bias.

3.2. Hamburg-ESO Survey for Bright QSOs

The Hamburg-ESO Survey for Bright QSOs is a survey that employs slitless spectroscopy on the ESO 1m Schmidt Telescope to find bright QSOs over an area that will eventually cover roughly $5000 \text{ } \square^\circ$ of the southern sky. See Wisotzki et al. (1996) and Reimers, Koehler & Wisotzki (1996) for details regarding the methods and techniques used in the development of this survey. Currently, a preliminary portion (roughly half) of the final dataset is available to the public. This subset contains 415 bright QSOs and Seyfert I nuclei with magnitudes in the range $13 \lesssim B_J \lesssim 17.5$ and redshifts $z < 3.2$ that span an effective area of roughly $3700 \text{ } \square^\circ$ (Wisotzki et al. 2000). Crowding of sources, especially on fields of low Galactic latitude, does result in the loss of spectra for roughly $\sim 30\%$ of the spectra on the fields. Nevertheless, the Hamburg-ESO survey QSO sample is particularly useful for this work because it is 99% spectroscopically complete over the well-defined ranges of magnitudes and redshifts given above and because it is devoid of redshift- and magnitude-related selection biases. The redshift distribution of Hamburg-ESO QSOs is shown as a dashed line histogram in Figure 2.

Though Hamburg-ESO QSOs were identified on plates containing slitless spectra corresponding to ESO/SRC field position (not the UKST), QSOs selected for this study were those whose positions lie within the 2.7° non-vignetted regions of the nearest respective UKST fields from which we had garnered our galaxy data. There is more overlap between UKST fields at high declinations than there is near the Celestial Equator. Therefore some high-declination QSOs lie within 2.7° degrees of multiple field centers. In these cases, we associated the QSO with the plate corresponding to the nearest field center. Those QSOs that lay further than 2.7° from any field center were not included in this study.

The QSOs that fall within the apparent magnitude range found in the Hamburg-ESO Catalogue are typically intrinsically brighter than M^* at most (especially at higher) redshifts. This implies that the catalogue samples the steep portion of the QSO number-magnitude count distribution and that one would expect to measure positive galaxy-QSO cross-correlations *à la* Equation 1.

4. Analysis

4.1. Estimation of the Correlation Function

The estimation of the galaxy-QSO cross-correlation is in many regards very similar to the determination of the galaxy auto-correlation, which has been conducted by many studies

in the past (Peebles 1980; Hewett, P. C. 1982; Maddox, Efstathiou & Sutherland 1996) and refinements have been incorporated in the technique (Hamilton 1993; Landy & Szalay 1993), but there are some notable differences as well.

Unlike autocorrelation estimates, the galaxy-QSO cross-correlation involves two separate catalogs, each with its own selection and window functions. In many cases, the selection function could also be an issue because one does not know *a priori* either the underlying galaxy or quasar distribution from which survey samples are obtained. Furthermore, the window function of a survey could also influence the correlation estimates by introducing geometrical effects that conspire with the sky densities of objects to skew correlation estimates relative to the values one would obtain from fair samples that very well characterize the true distributions of galaxies and QSOs.

An additional complication is the fact that the number of galaxies in our magnitude cuts from the APM catalogue is on the order of $\sim 10^4$ times greater than the number of QSOs in the Hamburg-ESO QSO catalogue. As a result, the uncertainty due to Poisson noise is greater relative to the signal for galaxy-QSO cross-correlations than it is for galaxy-galaxy auto-correlations.

A number of autocorrelation estimators can be found in the literature, including:

$$\omega_{GG1}(\theta) = \frac{DD}{\langle DR \rangle} - 1, \quad (2)$$

$$\omega_{GG2}(\theta) = \frac{DD \cdot \langle RR \rangle}{\langle DR \rangle^2} - 1, \quad (3)$$

$$\omega_{GG3}(\theta) = \frac{DD - 2\langle DR \rangle + \langle RR \rangle}{\langle RR \rangle}, \quad (4)$$

and

$$\omega_{GG4}(\theta) = \frac{DD}{\langle RR \rangle} - 1. \quad (5)$$

Here, D and R refer to whether the galaxies were drawn from direct or randomly generated samples, respectively, in order to generate the pair counts DD , DR and RR . Angled brackets represent averages over a large number of realizations (100 realizations in the case of this work) of the total pair counts between combinations of random (artificial) galaxies. Within each realization, we use a number of randomly generated objects as there are real objects in order to preserve normalization (this is true in the case of cross-correlations as well).

The most common estimator, ω_{GG1} , has largely replaced the original one, ω_{GG4} , in the literature and is often used in both auto- and cross-correlation (in a variant form) studies. This is because ω_{GG4} is most severely affected by window effects of the correlators mentioned here. It is a fact that has been known for quite some time, and has resulted in the

development of the newer correlation estimators, ω_{GG2} and ω_{GG3} , that Hamilton (1993) and Landy & Szalay (1993) developed in order to minimize the influence of contamination by the window and selection functions. These latter functions have the useful property that they are dependent on the galaxy-catalogue correlation function to higher orders than ω_{GG1} and should be less affected by selection and window effects as a result.

We have adapted these autocorrelation estimators for use in our cross-correlation study:

$$\omega_1(\theta) = \frac{D_G D_Q}{\langle D_G R_Q \rangle} - 1, \quad (6)$$

$$\omega_2(\theta) = \frac{D_G D_Q \langle R_G R_Q \rangle}{\langle D_G R_Q \rangle \langle R_G D_Q \rangle} - 1, \quad (7)$$

$$\omega_3(\theta) = \frac{D_G D_Q - \langle R_G D_Q \rangle - \langle D_G R_Q \rangle + \langle R_G R_Q \rangle}{\langle R_G R_Q \rangle}, \quad (8)$$

and,

$$\omega_4(\theta) = \frac{D_G D_Q}{\langle R_G R_Q \rangle} - 1, \quad (9)$$

where the subscripts G and Q indicate whether the direct or random samples represent galaxies or QSOs, respectively.

Like the galaxy autocorrelation estimators, each of the cross-correlation estimators are dependent to varying degrees on catalogue window functions and selection effects. Therefore, we have extended the formalism describing these dependencies found in Hamilton (1993) to the 2D auto- and cross-correlation estimators. Following the Hamilton (1993) formalism for a 2D catalogue, let us first define the catalogue selection function, Φ_x , which could be a function of object brightness, color, position, etc., for catalogue, x , which would be either $x = G$ or $x = Q$ for galaxies or QSOs, respectively. Unlike Hamilton (1993), we will assume that the positional dependence of Φ is 2-dimensional. If ν is the surface density of objects within a catalogue, then the total number of objects within the catalogue, x , can be determined with

$$N_{obs,x} = \Phi_x \nu_x, \quad (10)$$

so that if a catalogue contained all of the objects that lay within the bounds of the survey region, the selection function would be $\Phi = 1$. Φ is technically a discrete function, but it is entirely possible to treat it as a continuous function, especially with large numbers of catalogue objects.

If the catalogue window function is W_x , then w_x is defined so that

$$W_x \equiv w_x \Phi_x, \quad (11)$$

and the cross-pair window is

$$W_{GQ} = w_{GQ}\Phi_G\Phi_Q. \quad (12)$$

The pair weighting, w_{GQ} , need not be related to the point weightings, w_G and w_Q . Then the direct pair counts will involve $N_{obs,x}$, weighted by a function, w_x , and the direct-direct pair counts for cross-correlation analysis will be given by

$$D_G D_Q = w_{GQ} N_{obs,G} N_{obs,Q} = w_{GQ} \Phi_G \Phi_Q \nu_G \nu_Q, \quad (13)$$

while direct-random pairs will be given by either

$$D_G R_Q = w_{GQ} N_{obs,G} \Phi_Q = w_{GQ} \Phi_G \Phi_Q \nu_G \quad (14)$$

or by

$$R_G D_Q = w_{GQ} N_{obs,Q} \Phi_G = w_{GQ} \Phi_Q \Phi_G \nu_Q, \quad (15)$$

and finally the random-random pairs are given by

$$R_G R_Q = W_{GQ} = w_{GQ} \Phi_G \Phi_Q. \quad (16)$$

If $\bar{\nu}_G$ and $\bar{\nu}_Q$ are the mean sky surface densities of galaxies and QSOs lying within respective catalogue windows, then the degree to which they represent the true full-sky average surface density, $\bar{\nu}$, can be estimated with the sample overdensities σ_G and σ_Q , where

$$\bar{\sigma}_x = \frac{\bar{\nu}_x - \bar{\nu}}{\bar{\nu}} \quad (17)$$

for catalogue x . Fair samples that very well represent the true sky density of objects will have sample overdensities $\bar{\sigma}_x \approx 0$. Similarly, the object-catalogue correlation, ϕ_x , which is defined by either

$$\phi_G \equiv \frac{\langle W_{GQ} \sigma_G \rangle}{\langle W_{GQ} \rangle}, \quad (18)$$

or

$$\phi_Q \equiv \frac{\langle W_{GQ} \sigma_Q \rangle}{\langle W_{GQ} \rangle}, \quad (19)$$

should also be zero for a perfectly fair sample because the true object surface density in a sample, ν_x , would be equal to the true cosmic mean, $\bar{\nu}$.

Considering that the measured cross-correlation function will be, in general, a biased estimate of the true cross-correlation, we can define the windowed correlation,

$$\hat{\omega}_{GQ} \equiv \frac{\langle W_{GQ} \sigma_G \sigma_Q \rangle}{\langle W_{GQ} \rangle}, \quad (20)$$

which is equivalent to an unbiased cross-correlation in ideal circumstances.

The results, giving the correlators and their influence by the catalogue sample overdensities, $\bar{\sigma}_G, \bar{\sigma}_Q$, the catalogue-window correlations, ϕ_G, ϕ_Q , and the object-catalogue correlations, $\hat{\omega}_{GQ}$, are shown in Table 2. Additional estimators ($\omega_5 \dots \omega_7$) are also included. While these three estimators are not useful for determining the galaxy-QSO cross-correlations, they are helpful in gauging the degree to which randomly generated object distributions match real object distributions for modeling purposes. The most problematic terms in the third column of Table 2 are the first-order terms involving the catalogue-window correlations (the ϕ 's). It is then apparent that just like ω_{GG4} , the cross-correlation estimator, ω_4 , is inferior because of its greater dependence on the catalogue-window correlations, whereas ω_3 and ω_3 are only dependent on them to second order.

Direct pair counts were determined by counting all of the galaxies within angular separation bins $\theta \pm \frac{\delta\theta}{2}$ around QSOs, using galaxies that were taken from one field per QSO only. In addition to eliminating the effect of vignetting, this eliminates the need to account for plate to plate photometric sensitivity variations across the APM catalogue. Furthermore, all pairs were drawn from the inner $2\text{:}7$ portion of each UKST field. Though it does limit the angular scale over which we can estimate the cross-correlation to scales $\theta \leq 5\text{:}4$, this scale is rather large when compared to the scales over which prior studies have investigated and it prevents the contamination of the correlation signal by the plate to plate variations in the APM Catalogue photometric calibration and it serves to mitigate the influence of vignetting on the plate-density of galaxies.

The pair counts involving randomly generated QSOs and galaxies were also treated in a manner that limited the inclusion of geometric effects. For each QSO in our sample, 100 *Circularly-Distributed Random* (CDR) QSOs were generated that lay in a circle about the field center with a radius equal to the separation between the real QSO and the field center, and pair counts were averaged over the 100 realizations. Using CDR QSOs ensures that radial sensitivity gradients that may be present on the APM Schmidt plates cancel out, as will much of the edge effect introduced by the $2\text{:}7$ radius boundary. Random galaxies for use in determining the $\langle R_G R_Q \rangle$ and $\langle R_G D_Q \rangle$ terms that are found in the estimators ω_2, ω_3 and ω_4 were created by randomly scattering points on the field so that the probability of a random galaxy being generated at some spot on the field as equal for all points within $2\text{:}7$ of the field center and 0 outside that radius. The number of randomly generated galaxies and the number of real galaxies on the corresponding UKST field were the same in every realization in order to preserve normalization.

4.2. Angular Cross-Correlations

With combinations of pair counts in hand, we estimated the angular cross-correlations using each of the four estimators from the previous section with subsets of QSOs from a number of redshift bins of width $\Delta z = 0.2$ in the range $0 \leq z \leq 2$. This is the first time that all four of these cross-correlation estimators have been compared using the same QSO and galaxy data sets and each estimator gives very similar results in each subset. A typical comparison of each of the estimators and the magnitude of their respective RMS uncertainties is shown in Figure 3 using QSOs within a redshift range of 0.8 - 1. As expected, the greatest discrepancies between them are at the smallest and largest galaxy-QSO separations where the variance (also shown) is highest. At small separations, the variance is due largely to Poisson fluctuations in the small number of galaxies located very near QSOs while the rise in variance at large pair separations is due both to increasing relative Poisson uncertainties from the increasing importance of edge effects near the limiting separation scale of $5^\circ.4 = 324'$ of our study use the dispersion among the individual QSO estimates as a conservative measure of uncertainty rather than the error in the mean due to the possible presence of the various systematic effects that were mentioned in the previous section.

Among the individual correlators, $\omega_4(\theta)$, deviates the most from the others, especially at small and large separation scales where the stronger dependence of ω_4 on the window function becomes important. This is not surprising as ω_4 has long been considered an inferior estimator due to its relatively strong dependence on selection effects and window functions (Hamilton 1993). On the other hand, ω_1 , ω_2 , and ω_3 all yield very similar results across, which means that ω_1 is apparently still an acceptable choice. To be sure, Landy & Szalay (1993) and Hamilton (1993) have shown that ω_2 and ω_3 are less dependent on window and selection effects than ω_1 , but they also require significantly more computational time in order to sample the additional random galaxy population that ω_1 does not require. Hence if the cost of computation time exceeds the benefit of marginal signal improvement, then perhaps ω_1 would prove useful.

Furthermore, that each of the estimators, with their different dependences on the catalogue-object cross-correlations and relative over- or underdensity relative to the true object populations, are so similar implies that to a good degree both the APM galaxy catalogue and the Hamburg-ESO QSO catalogue are fair samples of their respective true object populations. This is significant because a number of earlier studies (see Table 1) that have used the APM galaxy catalogue have found significantly stronger cross-correlations than expected from models. If in some way, the APM did not represent a fair sample, statistical associations could conceivably result.

Finally, the angular cross-correlation measurements are quite significant. While it is

true that in the case of a single QSO on an APM field, the galaxy counts in adjacent annular separation bins will be correlated at some level because of the clustering of galaxies on the sky and because of sensitivity variations on the plate, this effect is likely small because we have seen that each of the different estimators yield similar results despite varying sensitivity to the underlying galaxy distribution. And while individual separation bins are only detected to 2σ on Figure 3, given that there are 415 QSOs in the Hamburg-ESO sample, which covers $3700 \text{ } \square^\circ$, the average separation between QSOs is $\sim 3^\circ$, so each of the small-separation angle bins should be nearly statistically independent because there should be little overlap of small-separation annuli around QSOs. As a result, considering that the small separation bins all show positive correlations and that they also follow an overall trend inconsistent with zero slope indicate that the detection of positive galaxy-QSO cross correlations is rather strong.

4.3. Cross-correlations vs. Source QSO Redshift

If the cross-correlations discussed in Section 4.2 are due to magnification bias, then their amplitudes should monotonically rise with increasing redshift beyond the lensing plane (at $z \approx 0.25$) (Dolag & Bartelmann 1997; Bartelmann & Schneider 2001; Ménard & Bartelmann 2002). We integrated the angular cross-correlations over scales up to 30 and 60' in order to increase the signal to noise ratio enough so that we could divide our QSO sample into a number of subsets based on QSO redshift and explore the z -dependence of the associations.

Figure 4 shows the integrated cross-correlation vs. redshift. Because of low QSO numbers per bin, we have used very wide ($\Delta z = 0.4$) redshift bins and we have therefore over-sampled to show the degree of variation with redshift. We do detect a positive signal on the order of 1 – 3% over all redshifts beyond the lens redshift, which is qualitatively consistent with magnification bias, and as expected, the Poisson noise is greater for the 30' plots than for the $\theta < 60'$ plot. This can be complicated by the integral constraint,

$$\frac{1}{\pi\theta^2} \cdot \int_0^{5.4} \omega(\theta) \cdot 2\pi\theta d\theta = 0. \quad (21)$$

Positive correlations at small separations must be balanced by negative correlations at higher separations.

Since the correlators were found to be very similar in the previous section, one would expect the same of the integrated estimators in Figure 4. This is generally the case, although the relative differences between the integrated estimators is a bit greater than the relative differences between the estimators themselves. Because

$$\omega(< \theta_o) = \frac{1}{\pi\theta_o^2} \int_0^{\theta_o} \omega(\theta) \cdot 2\pi\theta d\theta, \quad (22)$$

most of the signal contribution to $\omega(< \theta_o)$ comes from angular scales very near θ_o . Perhaps the differences between the integrated correlation function is then due to the modification of the angular correlation profile by the integral constraint. Minor differences between angular correlations on scales $\approx \theta_o$ would be exacerbated by the geometric scaling $\sim 2\pi\theta_o$.

The overlap between our galaxy and QSO samples at low redshift (Figure 2) means that the low redshift ($z \lesssim 0.4$) signal in Figure 4 is due to physical associations rather than magnification bias. The $\theta < 30'$ plot does in fact show a drop in the cross-correlation signal over redshifts in this range, along with a rise at redshifts greater than 0.4. This seems to indicate a fall off in the signal due to physical associations between galaxies and QSOs in front of the lensing plane, followed by an increase in the magnification bias signal involving QSOs beyond the lensing plane. The $\theta < 60'$ plot does not show a significant dip between the physical and lensing associations. Perhaps this is due to a combination of the oversampling in redshift and due to the integral constraint. Separations of $60'$ are of the same order of magnitude as the $5^\circ 4'$ limiting scale of our study and the integral constraint may be altering the correlations on these scales.

4.4. Confidence Tests

Individual angular cross-correlation functions from redshift bins with width $\Delta z = 0.4$ tend to be a bit noisy. Therefore, it is imperative to create a significance test for the integrated correlation function. Working toward this end, we have developed a Monte Carlo algorithm that generates a large number of realizations of the integrated cross-correlation measurements in the same manner as those from the last section. It utilizes our APM galaxy sample along with a large number of artificially generated QSO catalogues in order to determine the significance of the integrated correlation function measurements from the last section.

The algorithm works as follows: First, for each QSO in the Hamburg-ESO Catalogue, we generated one random QSO so that the probability lying at a particular point within 2.7 of the field center for this first type of QSO was equal for all points and 0 outside of that radius (as we did for our randomly generated galaxies, see Section 4.1). We shall call these *Uniformly-Distributed Random* (UDR) QSOs. Each UDR point was located on the same field as the real QSO that it replaced. Furthermore, in order to preserve the number of QSOs per redshift and magnitude bin, each was also attributed the same magnitude and redshift as the replaced real QSO. Next, for each UDR QSO, we generated 100 CDR QSOs (see Section 4.1) whose positions were distributed along a circle about the field center with a radius equal to the distance between the UDR QSO and the field center, as in our real-QSO

analysis. Finally, we determined the correlation function, ω_1 , from the resulting pair counts. This process was repeated 1000 times, effectively creating 1000 random realizations of the out cross-correlations. We interpret the distribution in values of the artificial cross-correlation functions to be indicative of the magnitude of the uncertainties in our measurement of the cross-correlation function.

Figure 4 shows the 50, 75, and 99% confidence limits that we derive from this interpretation, corresponding to the ranking of the values of 1000 cross-correlation realizations in each redshift bin. As the diagram indicates, the physical association signal is detected to high significance, especially in the lowest redshift bin, corresponding to source QSOs with redshifts ≤ 0.4 . The magnification bias signal seems to be most significantly detected in the $\theta < 30'$ frame at redshifts around 0.8 and 1.3, although the overall detection is somewhat marginal - with confidence levels on the order of 75%.

We do consider this Monte Carlo confidence analysis to be rather conservative, however. This is due to the fact that randomly generated QSOs can be either positively or negatively associated with APM galaxies and the confidence contours illustrate the ranking of individual realizations. The 99% contour therefore samples the very extremes of the underlying distribution. which seems to have a rather wide tail. Hence we believe the confidence limits are somewhat *underestimated*.

It is also useful to compare the galaxy-QSO results with those of cross-correlations between objects for which there should be no net cross-correlation. Therefore, we selected objects listed as stars in the APM catalogue with magnitudes $16 \leq R \leq 17.5$. Aside from the contamination of our stellar sample by galaxies on the faint side of our magnitude and object class cut, there is no reason that Galactic stars should be correlated in any way with QSOs that lie at cosmological distances. Figure 5 shows the strength of the integrated Star-QSO cross-correlation vs. redshift that was obtained in the same manner as the galaxy-QSO cross-correlation. No real dependence on redshift can be seen as each of the cross-correlation estimators oscillate above and below 0 in a manner that would be expected for random noise. Indeed, the star-QSO cross-correlation can serve to provide an independent indication of the noise level for the galaxy-QSO signal that is consistent with our Monte Carlo confidence estimate.

4.5. Modeling

We modeled the signal in Figure 4 based on a linear CDM large scale structure lensing model, given by Bartelmann & Schneider (2001), which gives the expected correlation

function from an assumed mass power spectrum. This particular model is a simplified version of that given by Dolag & Bartelmann (1997) in which an approximation is made by assuming that all galaxies are found at their median redshift. This approximation incurs errors on the order of 10%. The mass power spectrum used for our model was Case 1 obtained from the Appendix G of Bardeen et al. (1986) (BBKS): A CDM power spectrum with adiabatic fluctuations. We assumed a value of the present-day mass fluctuation normalization of $\sigma_8 = 1$, a matter density parameter of $\Omega_m = 0.3$, cosmological constant $\Omega_\Lambda = 0.7$, and expansion rate $h = 0.75$, resulting in a shape parameter of our modeled mass power spectrum was $\Gamma = 0.225$. The power spectrum at the lens plane redshift was then determined by scaling the present-day power spectrum with a factor of $(1 + z_{lens})^{-2}$.

Using our mass power spectrum and the assumption that all of the galaxies in our sample lie on a plane with a redshift $z = 0.25$, we determined the expected strength of the angular cross-correlations using the Bartelmann & Schneider (2001) approximation while varying the source redshift over the range represented by our QSO sample. Each of the correlation signals were integrated over separations up to 30 and 60', respectively. The model predicts an increase in the strength of the signal with source distance, provided that the sources lie behind the lensing plane. This can be seen in Figure 4, which agrees well qualitatively with the measured signal from the combination of Hamburg-ESO QSOs and APM galaxies. However, consistent with a large number of other studies (see the Introduction), the integrated modeled correlations were significantly lower (roughly a factor of 20) than our measured correlations. We will explore this further in the Discussion section.

4.6. Correlation scales

As we have mentioned earlier, we see in Figure 4 that QSOs with redshifts $z \lesssim 0.4$ are physically associated with the APM galaxy sample, while those at higher redshift are likely affected by magnification bias. We have separated our QSO sample into two redshift ranges in Figure 6, $z \leq 0.2$ and $0.6 \leq z \leq 1.0$, in order to see whether the differing assumed physical mechanisms result in different correlation functions. Outside of differences on angular scales greater than 130', the low and high redshift sample have very similar profiles. Both possess 'correlation lengths' (defined here as θ_o such that $\omega(\theta_o) = 0$, as opposed to the standard definition of the physical length, r_o , where $\xi(r_o) = 1$) of $\sim 110'$, which corresponds to scales of roughly 23 Mpc at the redshift of our APM galaxies ($z \approx 0.25$) (assuming $h = 0.75$). These scales are much larger than the typical sizes of groups and clusters and they seem to indicate that both physical and lensing associations are due to Large Scale Structure. That the physical and lensing associations have roughly the same correlation length may be due

to the fact that the same structure is likely responsible for both signals.

4.7. Galactic Dust

With such a large disagreement between the positive cross-correlations that are observed in this study with model expectations, it is appropriate to investigate whether these cross-correlations could in fact be generated by Galactic dust. If the QSOs in the Hamburg-ESO sample happen to lie in portions of the sky that are relatively unobscured by intervening Galactic dust, it could conceivably explain the amplitude discrepancy. Rodrigues-Williams & Hogan (1994) showed that the overdensity due to differences in levels of extinction, $\delta A_V(\theta)$, between two lines of sight separated by an angle, θ , is given by

$$q(\theta) = 10^{-2.5 \cdot \alpha_m \delta A(\theta)} \approx 1 - 5.76 \cdot \alpha_m \delta A(\theta). \quad (23)$$

If dust were the sole cause of the observed cross-correlations, then the maximal overdensity produced by dust would be roughly proportional to the differential extinction.

The Rodrigues-Williams & Hogan (1994) analysis determined the extremes in extinction across LBQS fields using the Burstein & Heiles (1982) maps and found that the observed galaxy-QSO cross-correlations between LBQS QSOs and APM galaxies were in fact anti-correlated with the cross-correlations that would have been expected if they were due solely to Galactic extinction.

We used a slightly different technique in which we interrogated the Schlegel, Finkbeiner & Davis (1998) Galactic $E(B - V)$ reddening maps using the IDL `dust_getval` routine, which is provided by Schlegel & Finkbeiner (1999), to derive and compare the differences in extinction levels between Hamburg-ESO QSO positions and large-scale averages within surrounding annuli with inner and outer radii of 135' and 150', respectively. We define the differential extinction by

$$\delta A_V(\theta) = A_V(< 15') - A_V(135 - 150'). \quad (24)$$

The Schlegel, Finkbeiner & Davis (1998) reddening map has a resolution of $6^m1 \times 6^m1$ and local reddening values were interpolated from the adjacent surrounding pixels. We determined extinction levels from the Schlegel, Finkbeiner & Davis (1998) reddening map by adopting a single value for the ratio of total to selective extinction $R_V = 3.1$ for every Hamburg-ESO QSO.

Meanwhile, we determined the galaxy number densities from the same regions and

measured the relative overdensities between the QSO positions and the field:

$$q = \frac{N(< 15')}{N(135 - 150')}. \quad (25)$$

The reason for the specific choice of the annular region size was that it represents the approximate angular scale at which the galaxy-QSO cross-correlations, $q(\theta) - 1 = \omega(\theta)$ are near zero for our sample. Figure 7 shows that the relative overdensities and the differential extinctions between the QSO positions and the field are uncorrelated. In addition, the solid, dotted and dashed lines in Figure 7 show the maximal overdensities that would be expected from dust extinction alone, given slopes of $\alpha_m = 0.6, 0.4$, and 1.0 , respectively. The slope of 0.6 corresponds roughly to the slope of the QSOs in our sample, while 0.4 corresponds to the critical slope at which there would be no expected lensing signal. If dust were the sole cause of the cross-correlation signal, one would expect that the magnitude of the overdensities (underdensities) would lie somewhere between a value of $q = 1$ and the curve derived using the appropriate QSO sample slope. Yet, the most of the QSO overdensities fall outside this bound.

5. Discussion and Conclusions

An important result of this work is the detection of a net positive correlation signal over the entire redshift range for which we have significant numbers of QSOs (see Figures 3 and 6). Though our Monte Carlo simulations suggest a modest level of confidence for the integrated correlations, our having detected a consistently positive signal over all redshift intervals suggests that perhaps a somewhat higher level of confidence could be placed on the result. The Monte Carlo results also belie the fact that the *angular* cross-correlations from various redshift intervals are quite significant and that they indicate strong detections of positive galaxy-QSO cross-correlations. We anticipate that when the final Hamburg-ESO QSO Catalogue is finished, effectively doubling the size of the current sample, the total S/N ratio should in principle improve by a factor of roughly $\sqrt{2}$, which would lend a significantly higher level confidence in the cross-correlation measurements.

The measurements of statistical associations between APM galaxies and Hamburg-ESO QSOs occur on angular scales $\theta \lesssim 110'$. The overall shape of the correlations for physical and lensed associations are very similar. Meanwhile, the correlation length (equivalent for both types of associations, corresponding to ~ 20 Mpc scales at $z_{lens} \approx 0.25$) suggests that large scale structure is doing the lensing rather than more compact objects such as galaxy clusters.

Despite the large order of magnitude discrepancy between our modeled and observed

integrated cross-correlation functions, we are consistent with several other studies, including Benítez & Martínez-González (1997); Williams & Irwin (1998); Norman & Williams (2000) and Benítez et al. (2001), because they have also noted such large discrepancies. A number of potential causes for the mismatches have been discussed in the literature. On small angular scales less than a few arcminutes, correlations can be explained by the halo model, which indicates that the strength of the signal is very dependent on the halo occupation properties of various types of galaxies. Depending on the specific types of galaxies used, the halo model predicts an enhancement of a factor of 2 - 10 on small angular scales relative to nonlinear clustering models by Bartelmann (1995) and Dolag & Bartelmann (1997) (Jain, Scranton & Sheth 2003). There is still a discrepancy on the $\gtrsim 30'$ scales within this study, however, and a number of other phenomena have been investigated to explain this. Williams (2000), for example, investigated extending lensing formalism by including higher order general relativistic terms, but this results only in a $\sim 10\%$ increase in the theoretical cross-correlation estimate. Many other studies have suggested dust, but extragalactic dust would tend to reduce cross-correlation, but there is probably little or no dust in clusters (Nollenberg et al. 2003). Galactic dust could create positive correlations, but one would also expect to see positive correlations between faint stars and QSOs, which we do not detect. Studies involving radio-selected QSOs (see Table 1), which should be unaffected by dust, are also inconsistent with significant amounts of Galactic obscuration. We have also compared various cross-correlation estimators. Each are dependent to varying degrees on selection effects and window functions, but each yield very similar results. This likely implies that at least the APM and Hamburg-ESO catalogues are fair samples of their respective populations and that systematic effects are not inflating the cross-correlation estimates.

So in order to further investigate the discrepancy between the model and the observations, we have also measured the slope of the QSO number-magnitude counts, α_m , as a function of redshift using the same sample of QSOs for each redshift bin that was described in Section 4.3 (the binwidth is, again, $\Delta z = 0.4$). Figure 8 shows that α_m is indeed above the critical value of 0.4 for all redshifts, with perhaps a slight overall increase in the slope with increasing QSO redshift. Typical values are on the order of $\alpha_m \approx 0.6$. The error bars represent the 1σ RMS variation in the slope of $\Delta z = 0.1$ subsets of the $\Delta z = 0.4$ bins of our QSO sample and uncertainties at redshifts $z > 1.5$ are underestimated due to low QSO numbers.

Using the measured α_m with the measured correlation strengths, we determined the degree of magnification present, assuming that the signal is due to magnification bias (see Equation 1). The magnification is plotted vs. measured correlation strength in Figure 9, using the same data found in Figures 4 and 8. Because the physical associations do not obey Equation 1, the estimated magnification should not necessarily compare with that expected

from the magnification bias affect points. Therefore, we are able to separate those points corresponding to low-redshift physical associations from the lensed points at higher redshift with this plot.

Finally, because of the rather large amplitude discrepancy with the models, we investigated whether the observed overdensities could be due to extinction by Galactic dust. As mentioned in Section 4.7, there is no correlation between the measured galaxy overdensities about the QSOs and the differences in extinction level between the QSO lines of sight and the field. If dust were the cause, one would have difficulty in explaining the observed underdensities that have been measured in other studies that employ faint QSOs, as expected from magnification bias. Patchy Galactic dust can only produce positive cross-correlations, not anti-correlations. Both of these lines of evidence suggest that Galactic dust is not the cause of the large amplitude in the cross-correlation signal. Furthermore considering that the signal appears to behave as expected, qualitatively, for magnification bias, it seems likely that this is the cause of the observed galaxy-QSO cross-correlations.

Yet we are still left with the long-standing problem of the discrepancy with models. There remain a number of avenues to explore in hopes of solving this problem. Dust, whether Galactic or extragalactic in origin, are unlikely to skew the values of the cross-correlations significantly. Galactic dust is incapable of explaining anti-correlations and extragalactic dust can not result in positive correlations. Both types of correlations are observed in accordance to magnification bias. We will investigate the effect of catalogue masks and selection effects in Nollenberg & Williams (2005), though there are still a number of other places to look for a solution. For example, perhaps models need to account for multiple or nonlinear deflections for a given light ray as it travels from source to observer. There has also been a suggestion by Bassett and Kunz that since galaxy-QSO cross-correlations are one of two types of studies (the other involving Type-Ia supernovae) in which both the luminosity and angular diameter distances are sampled, there may be an asymmetry between the two distances (Bassett & Kunz 2003, 2004). This asymmetry could in principle be caused by essentially any process that would hinder a photon from reaching an observer, including Compton scattering off the ionized IGM or something much more exotic such as photon decay.

We thank Lutz Wisotzki for his provision of the initial release of the Hamburg-ESO QSO catalogue and for his very useful comments regarding the preparation of the survey and his equally helpful suggestions for this paper.

REFERENCES

- Annis & Jewitt, 1993, MNRAS, 264, 593
- Arnaud, K. A. & Mushotzky, R. F., 1998, ApJ, 501, 119
- Bahcall, N. A., in *Formation of Structure in the Universe*, eds. Dekel, A. & Ostriker, J. P., (Cambridge University Press: Cambridge), p.135 - 171 and references therein
- Bardeen, J. M., Bond, J. R., Kaiser, N. & Szalay, A. S., 1986, ApJ 304, 15
- Bartelmann, M., 1995, A&A, 298, 661
- Bartelmann, M. & Schneider, P., 1993, A&A, 271, 421
- Bartelmann, M. & Schneider, P., 1994, A&A, 284, 1
- Bartelmann, M. & Schneider, P., 2001, Phys. Rep., 340, 291
- Bartsch, A., Schneider, P. & Bartelmann, M., 1997, A&A, 319, 375
- Bassett, B. & Kunz, M., 2003, astro-ph/0312443
- Bassett, B. & Kunz, M., 2004, ApJ 607, 661
- Baugh, C. M. & Efstathiou, G., 1993, MNRAS 265, 145
- Benítez, N. & Martínez-González, E., 1995, ApJ 448, L89
- Benítez, N. & Martínez-González, E., 1997, ApJ 477, 27
- Benítez, N., Sanz, J. L. & Martínez-González, E., 2001, MNRAS 320, 241
- Biviano, A., Giurcin, G., Mardirossian, M. & Rephaeli, Y., 1990, in *Dusty Objects in the Universe*, eds. E. Bussoletti & A. A. Vittone, Kluwer Academic Publishers
- Borgeest, U., von Linde, J. & Refsdal, S. 1991, A&A, 251, L35
- Boyle, B. J., Fong, R. & Shanks, T., 1988, MNRAS 231, 897
- Broadhurst, T. J., Ellis, R. S. & Shanks, T., 1988, MNRAS 235, 827
- Burstein, D. & Heiles, C. 1982, AJ, 87, 1165
- Canizares, C. R., 1981, Nature, 291, 620
- Colless, M. M., Ellis, R. S., Taylor, K. & Hook, R. N., 1990, MNRAS 244, 408

- Colless, M. M. et al., 1993, MNRAS 261, 19
- Croom, S. M. & Shanks, T., 1999, MNRAS, 307, L17
- Dolag, K. & Bartelmann, M., 1997, MNRAS, 291, 446
- Drinkwater et al., 1992, Proc. ASA, 10, 1
- Dwek, E., Rephaeli, Y. & Mather, J. C. 1990, ApJ, 350, 104
- Ferguson, H., 1993, MNRAS, 263, 343
- Fugmann, W., 1988, A&A, 204, 73
- Fugmann, W., 1990, A&A, 240, 11
- Gaztañaga, E. 2003, ApJ, 589, 82
- Hamilton, A. J. S., 1993, ApJ, 417, 19
- Hammer, F. & Le Fèvre, O., 1990, ApJ, 357, 38
- Hewett, P. C., 1982, MNRAS, 201, 867
- Hewett, P. C., Foltz, C. B. & Chaffee, F. H., 1995, AJ, 109, 1498
- Hewitt, A. & Burbidge, G., 1980, ApJS, 43, 57
- Hewitt, A. & Burbidge, G., 1981, ApJS, 46, 113
- Hintzen, P., Romanishin, W. & Valdes, F., 1991, ApJ, 366, 7
- Hu, E. M., ApJ, 391, 608
- Irwin, M., *APM cat*, 1996, <http://www.ast.cam.ac.uk/apmcat>
- Jain, B., Scranton, R. & Sheth, R. K., 2003, MNRAS, 345, 62
- Karachentsev, I. D. & Lipovetskii, V. A., 1969, Soviet Phys., 12, 909
- Landy, S. D., Szalay, A. S., 1993, ApJ, 412, 64
- Loveday, J., Peterson, B. A., Efstathiou, G., & Maddox, S. J., 1992a, ApJ 390, 338
- Loveday, J., Efstathiou, G., Peterson, B. A. & Maddox, S. J., 1992b, ApJ 400, L43
- Maddox, S. J., Efstathiou, G. & Sutherland, W. J., 1996, MNRAS 283, 1227

- Maoz, D. 1995, ApJ, 455, L115
- Ménard, B. & Bartelmann, M., 2002, A&A, 386, 784
- Myers et al., 2003, MNRAS 342, 467
- Nollenberg, J. G., Williams, L. L. R. & Maddox, S. J., 2003, AJ, 125, 2927
- Nollenberg, J. G., Williams & L. L. R., 2005, *in prep*
- Norman, D. J. & Impey, C. D., 1999, AJ, 118, 613
- Norman, D. J. & Williams, L. L. R., 2000, AJ, 119, 2060
- Peebles, P. J. E., 1980, "The Large Scale Structure of the Universe", Princeton University Press
- Reimers, D., Koehler, T. & Wisotzki, L., 1996, A & AS, 115, 235
- Rodrigues-Williams, L. L. R. & Hogan, C. J., 1994, AJ, 107, 451
- Romani, R. W., Maoz, D. 1992, ApJ, 386, 36
- Schlegel, D. J., Finkbeiner, D. P. 1999, <http://astron.berkeley.edu/davis/dust>.
- Schlegel, D. J., Finkbeiner, D. P. & Davis, M. 1998, ApJ, 500, 525
- Seitz, S. & Schneider, P., 1995, A&A, 302, 9
- Thomas, P. A., Webster, R. L. & Drinkwater, M. J., 1995, MNRAS, 273, 1069
- Turner, E. L., 1980, ApJ, 242, L135
- Tyson, A. J., 1986, AJ, 92, 691
- de Vaucouleur, G., de Vaucouleur, A. & Corwin, H. G. Jr., 1972, AJ, 77, 4, 285
- Véron-Cetty, M.-P. & Véron, P., 1989, *A Catalogue of Quasars and Active Nuclei* (4th Ed., Garching: ESO)
- Voit, G. M. & Donahue, M. 1995, ApJ, 452, 164
- Webster, R. L. et al., 1988, Nature, 336, 358
- Williams, L. L. R., 2000, ApJ, 535, 37
- Williams, L. L. R. & Irwin, M. J., 1998, MNRAS, 298, 378

Wise, M. W., I'Connel, R. W., Bregman, J. N. & Roberts, M. S., 1993, ApJ, 405, 94

Wisotzki, L., 2000 A & A, 353, 861

Wisotzki, L., et al., 2000, A & A, 358, 77

Wisotzki, L., Koehler, T., Groote, D. & Reimers, D., 1996, A & AS, 115, 227

Zwicky, F., *Problems of Extragalactic Research.*, ed. G. C. McVittie (New York: Macmillan),
p. 149

Table 1. Previous Results from Galaxy-QSD Association

Study	Galaxy Source	Galaxies Mag/Flux	QSO Source	QSOs Mag/Flux	QSO Redshifts	Angular Scales	Detected
Tyson (1986)	Tyson (1986)	$R \lesssim 21$	Hewitt & Burbidge (1980)	$17 < V < 20$	$0.13 - 0.48$	$< 30''$	+
	"	"	"	"	$0.96 - 1.5$	"	+
Webster et al. (1988)	APM UKST	$B_J < 21$	Webster et al. (1988)		$1 - 3$	$\lesssim 10''$	+
Fugmann (1988)	Fugmann (1988)	$r < 21^m5$	1 Jy Flat spectrum QSOs	$S_{5GH_z} \geq 1\text{Jy}$	$z > 1.7$	$< 60''$	+
Fugmann (1990)	Lick Catalogue	$m_{pg} < 18^m9$	1 Jy Flat spectrum QSOs	$S_{5GH_z} \geq 1\text{Jy}$	$z \geq 1$	$\sim 10'$	+
	"	"	"	"	$0.2 - 1$	"	0
Hammer & Le Fèvre (1990)	Hammer & Le Fèvre (1990)	$R \leq 21$	3CR radio galaxies	$S_{178MHz} : 4.5 - 9\text{Jy}$	$z \geq 1$	$\sim 5''$	+
Hintzen et al. (1991)	Hintzen et al. (1991)	$R < 21$	Véron-Cetty & Véron (1989)	$17 < V < 20$	$0.9 - 1.5$	$\sim 15''$	+
Drinkwater et al. (1992)	Drinkwater et al. (1992)	$V < 18^m0$	Drinkwater et al. (1992)	$16 \leq V \leq 18$	$0.7 - 2.5$	$15''$	+
Bartelmann & Schneider (1994)	IRAS Faint Source Cat.	$S_{60\mu m} : 0.3 - 1\text{Jy}$	1 Jy Flat spectrum QSOs	$S_{5GH_z} \geq 1\text{Jy}$	$z \gtrsim 1.25$	$\sim 10'$	+
Boyle, Fong & Shanks (1988)	APM UKST	N/A	UVX	$B < 20^m0$	< 2.2	$< 10'$	-
Rodrigues-Williams & Hogan (1994)	Zwickey Clusters	N/A	LBQS	$B \leq 18^m5$	$1.4 - 2.2$	$\gtrsim 140'$	+
Benítez & Martínez-González (1997)	COSMOS/UKST	$B_J \lesssim 21$	LBQS	$B_J < 20.5$	$0.3 - 4$	$< 15'$	-
Williams & Irwin (1998)	APM UKST	$16 \leq R \leq 20.46$	LBQS	$B_J \leq 18^m0$	$< 100'$	< 3.3	+
Croom & Shanks (1999)	COSMOS/UKST	$B_J < 20.5$	UVX	$17.9 < B < 20.65$	$0.3 - 2.2$	$< 10'$	-
Gaztañaga (2003)	SDSS	$r' = 19 - 22$	SDSS	$i' < 19.1$	$0.8 - 2.5$	$< 10'$	+
Myers et al. (2003)	APM and SDSS	$B < 20.5$	2dF	$B < 20.5$	< 3	$\gtrsim 10'$	-
Seitz & Schneider (1995)	Zwickey Clusters	N/A	1 Jy Catalogue	$S_{5GH_z} > 1\text{Jy}$	$0 - 0.5$	$\gtrsim 15'$	+
Seitz & Schneider (1995)	Zwickey Clusters	N/A	1 Jy Catalogue	$S_{5GH_z} > 1\text{Jy}$	$0.5 - 1.5$	$\gtrsim 15'$	-
Benítez & Martínez-González (1997)	COSMOS/UKST	$B_J \lesssim 21$	Parks catalogue	$S_{11cm} > 0.5\text{Jy}$	$0.3 - 4$	$< 15'$	+
Norman & Williams (2000)	APM UKST	$18.5 < R < 20$	1 Jy Catalogue	$S_{5GH_z} > 1\text{Jy}$	> 0.5	$< 60'$	+
Benítez et al. (2001)	COSMOS/UKST	$B_J < 20.5$	1 Jy Catalogue	$S_{5GH_z} > 1\text{Jy}$	< 3	$< 15'$	+
Benítez et al. (2001)	COSMOS/UKST	$B_J < 20.5$	0.5 Jy Catalogue	$S_{5GH_z} > 0.5\text{Jy}$	< 3	$< 15'$	+

Table 2: 2D Estimator dependence on catalogue characteristics

Correlator	Pair counts	Dependence
Autocorrelation estimators		
ω_{GG1}	$\frac{DD}{\langle DR \rangle} - 1$	$\frac{\hat{\omega}_{GG} + \phi_G - \bar{\sigma}_G - \phi_G \bar{\sigma}_G}{(1 + \phi_G)(1 + \bar{\sigma}_G)}$
ω_{GG2}	$\frac{DD \cdot \langle RR \rangle}{\langle DR \rangle^2} - 1$	$\frac{\hat{\omega}_{GG} - \phi_G^2}{(1 + \phi_G)^2}$
ω_{GG3}	$\frac{DD - 2\langle DR \rangle + \langle RR \rangle}{\langle RR \rangle}$	$\frac{\hat{\omega}_{GG} - 2\phi_G \bar{\sigma}_G + \bar{\sigma}_G^2}{(1 + \bar{\sigma}_G)^2}$
ω_{GG4}	$\frac{DD}{\langle RR \rangle} - 1$	$\frac{\hat{\omega}_{GG} + 2\phi_G - 2\bar{\sigma}_G - \bar{\sigma}_G^2}{(1 + \bar{\sigma}_G)^2}$
ω_{GG5}	$\frac{\langle DR \rangle}{\langle RR \rangle} - 1$	$\frac{\phi_G - \bar{\sigma}_G}{(1 + \bar{\sigma}_G)}$
Cross-correlation estimators		
ω_1	$\frac{D_G D_Q}{\langle D_G R_Q \rangle} - 1$	$\frac{\hat{\omega}_{GQ} + \phi_Q - \bar{\sigma}_Q(1 + \phi_G)}{(1 + \phi_G)(1 + \bar{\sigma}_Q)}$
ω_2	$\frac{D_G D_Q \cdot \langle R_G R_Q \rangle}{\langle D_G R_Q \rangle \langle R_G D_Q \rangle} - 1$	$\frac{\hat{\omega}_{GQ} - \phi_G \phi_Q}{(1 + \phi_G)(1 + \phi_Q)}$
ω_3	$\frac{D_G D_Q - \langle D_G R_Q \rangle - \langle R_G D_Q \rangle + \langle R_G R_Q \rangle}{\langle R_G R_Q \rangle}$	$\frac{\hat{\omega}_{GQ} - \phi_G \bar{\sigma}_Q - \phi_Q \bar{\sigma}_G + \bar{\sigma}_G \bar{\sigma}_Q}{(1 + \bar{\sigma}_G)(1 + \bar{\sigma}_Q)}$
ω_4	$\frac{D_G D_Q}{\langle R_G R_Q \rangle} - 1$	$\frac{\hat{\omega}_{GQ} + \phi_G - \bar{\sigma}_G + \phi_Q - \bar{\sigma}_Q + \bar{\sigma}_G \bar{\sigma}_Q}{(1 + \bar{\sigma}_G)(1 + \bar{\sigma}_Q)}$
ω_5	$\frac{\langle D_G R_Q \rangle}{\langle R_G R_Q \rangle} - 1$	$\frac{\phi_G - \bar{\sigma}_G}{(1 + \bar{\sigma}_G)}$
ω_6	$\frac{\langle R_G D_Q \rangle}{\langle R_G R_Q \rangle} - 1$	$\frac{\phi_Q - \bar{\sigma}_Q}{(1 + \bar{\sigma}_Q)}$
ω_7	$\frac{D_G D_Q}{\langle R_G D_Q \rangle} - 1$	$\frac{\hat{\omega}_{GQ} + \phi_G - \bar{\sigma}_G(1 + \phi_Q)}{(1 + \bar{\sigma}_G)(1 + \phi_Q)}$

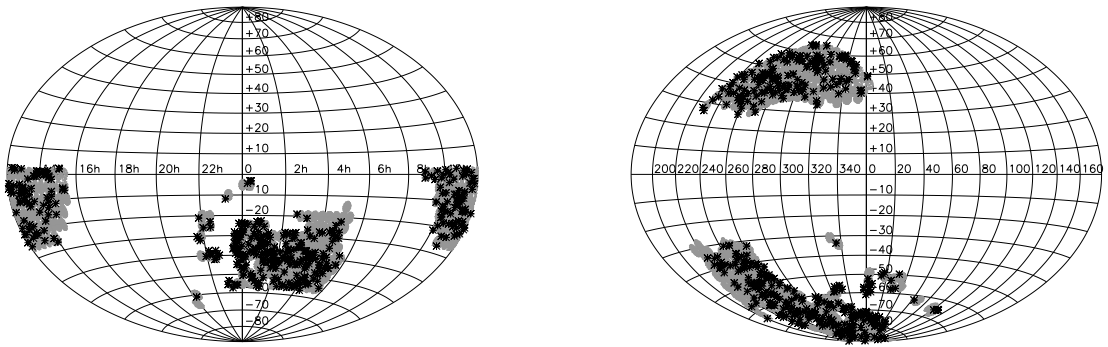


Fig. 1.— Sky positions of APM galaxies (grey points) and Hamburg-ESO QSOs (black asterisks) used in this study. *Left*: Equatorial coordinates. *Right*: Galactic coordinates.

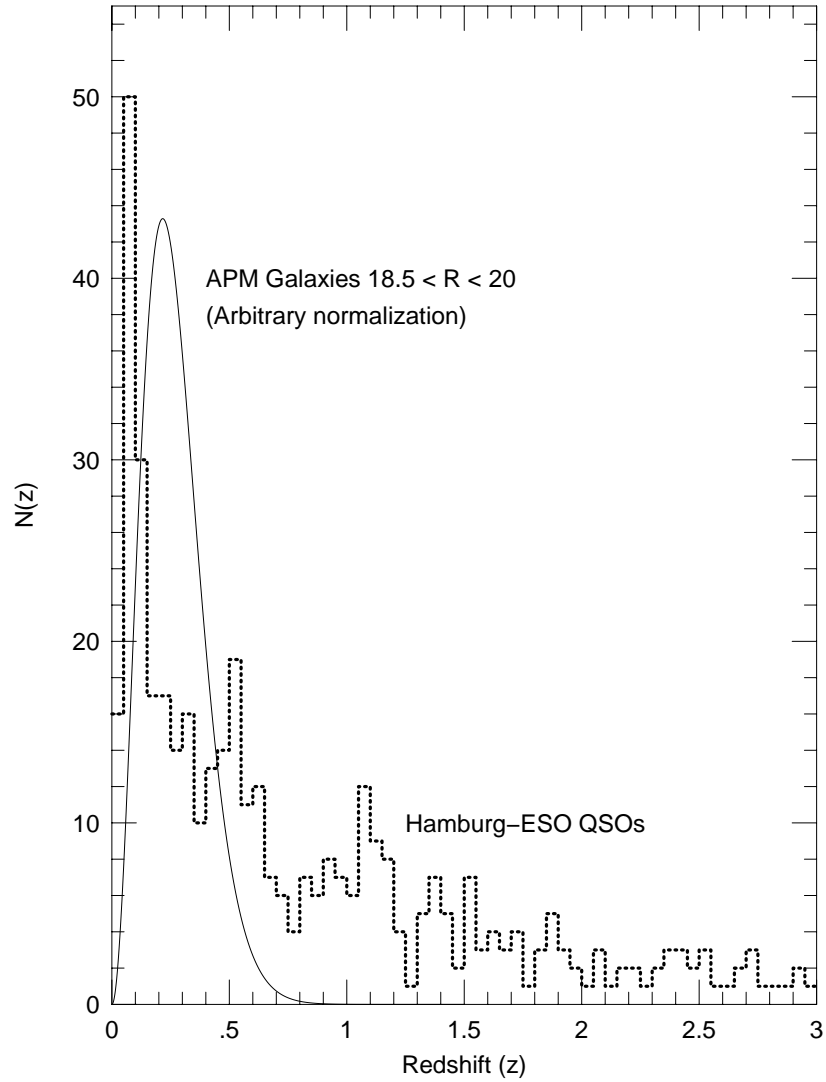


Fig. 2.— Redshift distributions of Galaxies and QSOs used in this study. The histogram represents the QSOs in the Hamburg-ESO QSO sample while the solid line shows the estimated redshift distribution (with arbitrary normalization) for our sample of roughly $4.5 \cdot 10^6$ APM Galaxies with magnitudes $18.5 \leq R \leq 20$, following Maddox, Efstathiou & Sutherland (1996).

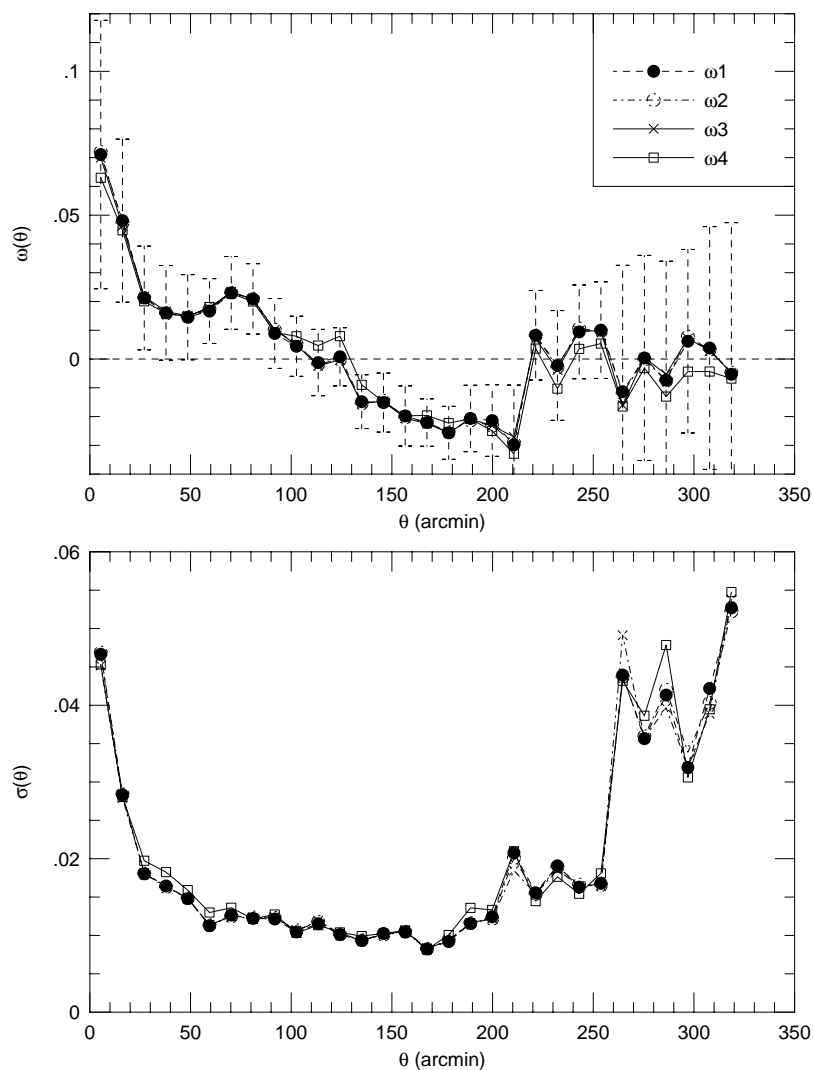


Fig. 3.— A comparison between correlation function estimators, using a sample of QSOs with redshifts $0.8 < z < 1.0$ and magnitudes $B_J \leq 17.5$. *Top*: Angular correlation function vs. pair separation angle. The correlators ω_1, ω_2 and ω_3 are very similar in this case. *Bottom*: RMS Uncertainty in the correlation function calculated using the distribution of correlation functions of individual QSOs within the sample. The errorbars in the top panel show the RMS uncertainty for ω_1 .

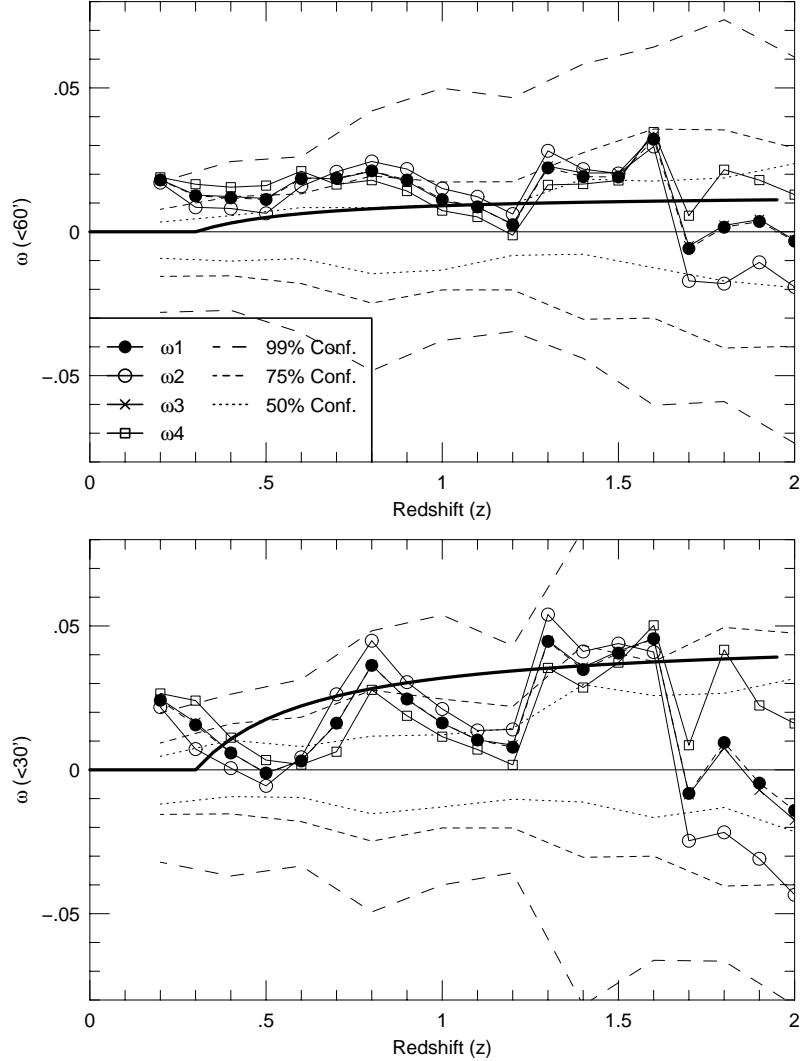


Fig. 4.— Measured and modeled integrated correlation functions vs. redshift with confidence limits. Each of the four correlation estimators from the Methods section are shown. *Top:* Correlation functions integrated over separations $\leq 60'$. *Bottom:* The same, but now integrated over separations $\leq 30'$. The bold dark line in each case represents a large scale structure lensing model with a linear CDM mass power spectrum, following Bartelmann & Schneider (2001). Dotted, dashed and long-dashed lines represent 50, 75 and 99% confidence limits from 1000 iterations of our monte carlo error estimation. Note the positive signal detected at redshifts $z > 0.25$ and that ω_3 nearly coincides with ω_1 on both panels.

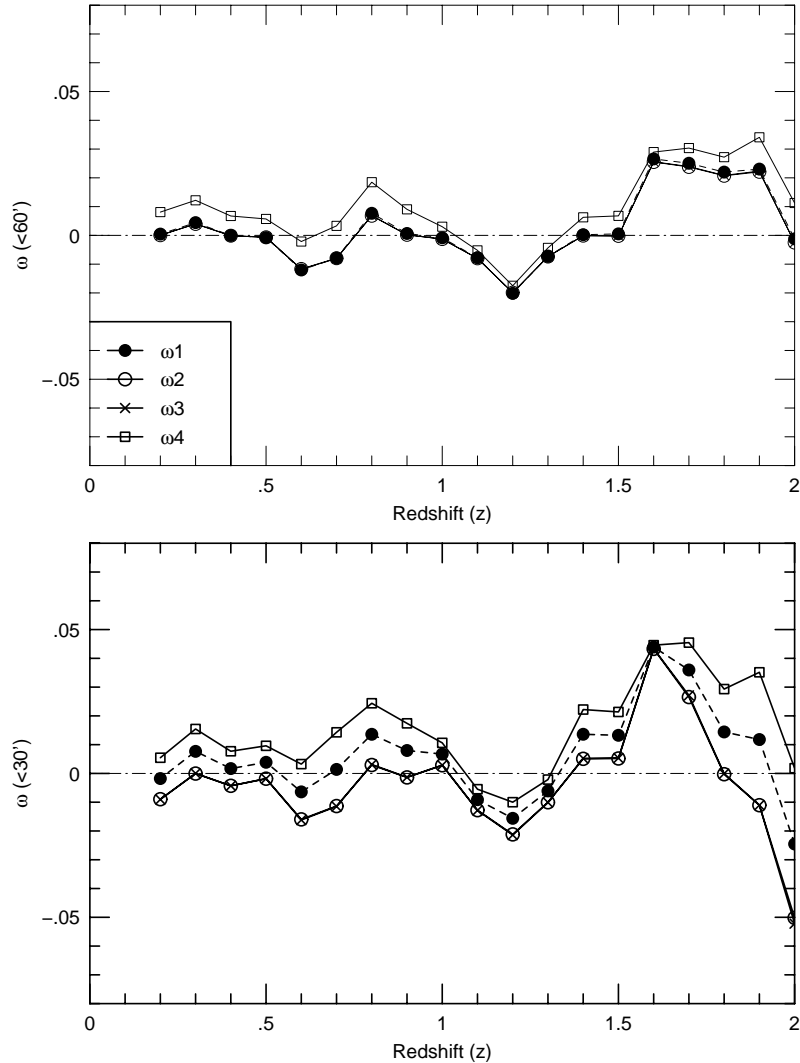


Fig. 5.— Same as Figure 4 only substituting galaxies with a selection of APM stars with magnitudes between $16 \leq R \leq 17.5$. One would expect no correlation between stars and distant QSOs. Unlike the positive signal seen in Figure 4, we indeed find no correlation between stars and QSOs. Offsets between the various estimators are due to differing shapes of the individual correlation functions from each estimator. Some contamination of the stellar sample by galaxies is possible. Several estimators are in close agreement for the $60'$ correlations while ω_2 and ω_4 are most similar in $30'$ correlations.

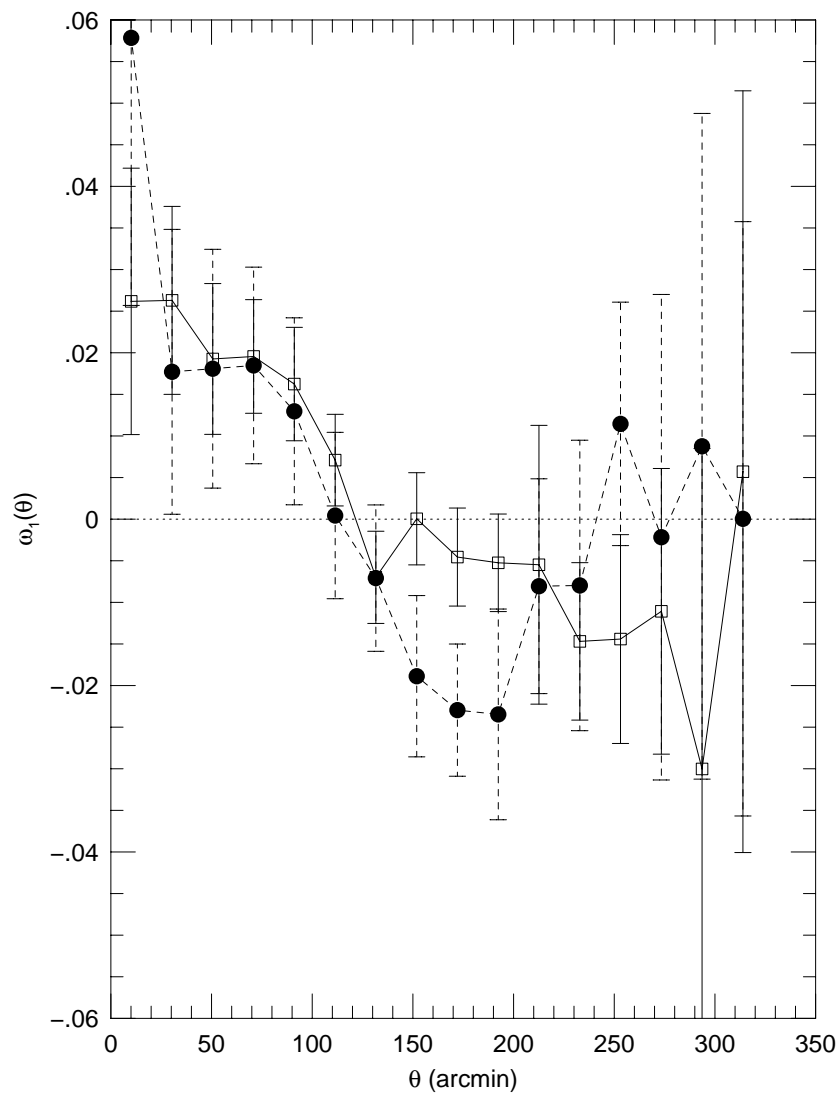


Fig. 6.— Correlation functions from two redshift cuts. *Empty Squares*: All 113 QSOs with $0 < z < 0.2$ (physical associations). *Solid dots*: The 79 QSOs with $0.6 < z < 1.0$, corresponding to the location of the strongest signal in the integrated correlations from Figure 4 (magnification bias). Despite their different physical cause, both correlation functions appear to be very similar considering the statistical uncertainties.

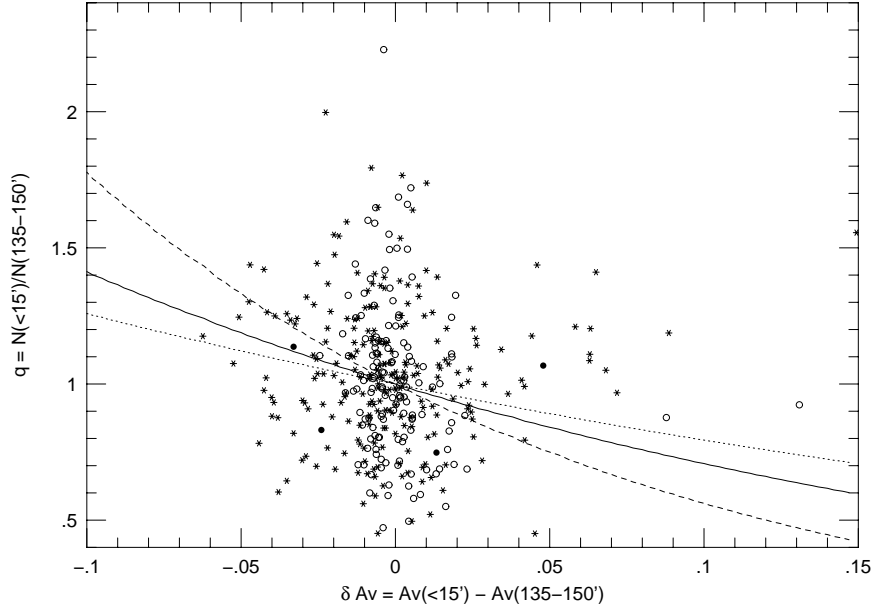


Fig. 7.— The observed overdensities of galaxies within 15' of QSOs with respect to galaxies between 135 – 150' is plotted here versus the difference in Galactic extinction between the same separation scales. The points are divided between high- (60 - 90°), mid- (30 - 60°), and low-Galactic Latitude (0 - 30°) samples (empty circles, stars, and filled circles, respectively). The points appear completely uncorrelated. In addition the expected maximal overdensities are plotted as a function of differential extinction for cases in which the QSO cumulative number-magnitude count slope $\alpha_m = 0.6$ (solid), 0.4 (dotted), and 1.0 (dashed). (See Equation 23.)

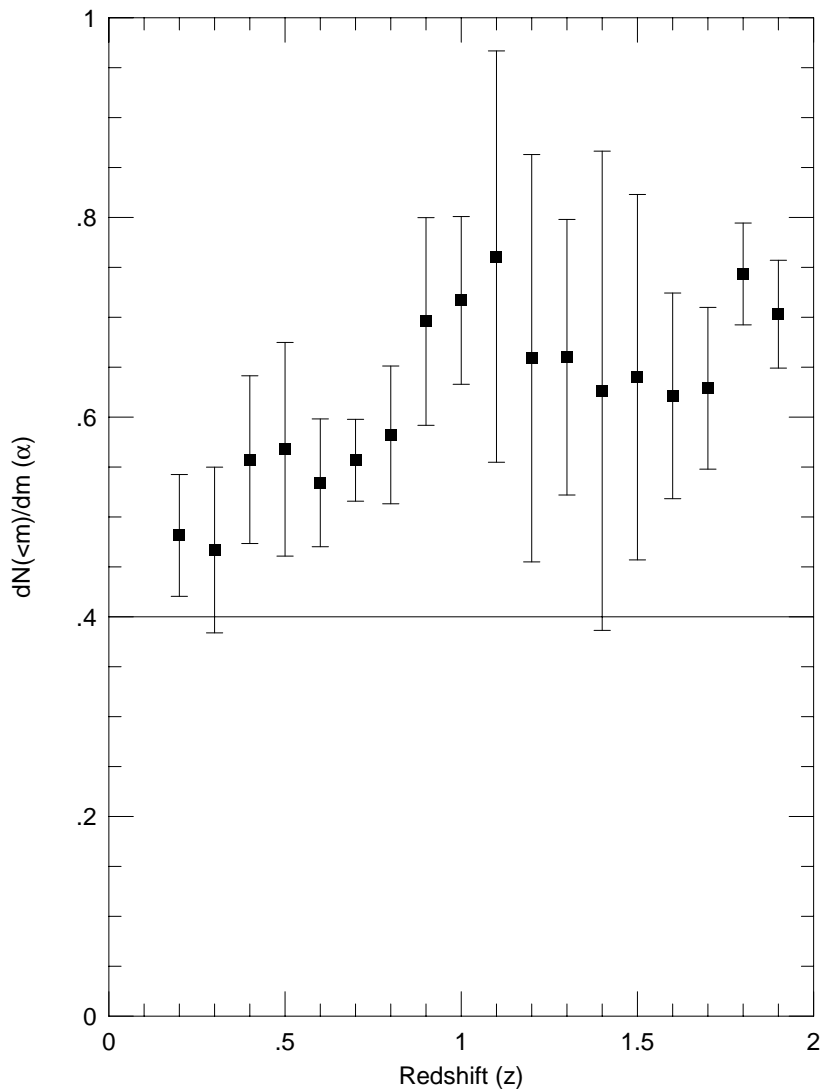


Fig. 8.— Average slope of the QSO number-magnitude counts plotted vs. redshift. Redshift bins have width $\Delta z = 0.4$ and each bin contains the same QSOs as the bins found in Figure 4. The value of the slope of the QSOs within the Hamburg-ESO Catalogue is $\alpha_m > 0.4$ for all redshifts, implying the expectation of positive correlations due to magnification bias. Error bars represent the 1σ RMS of slopes from subsets of the data. Uncertainties given at redshifts between $1.5 \leq z \leq 2.0$ are artificially low due to low QSO numbers per bin.

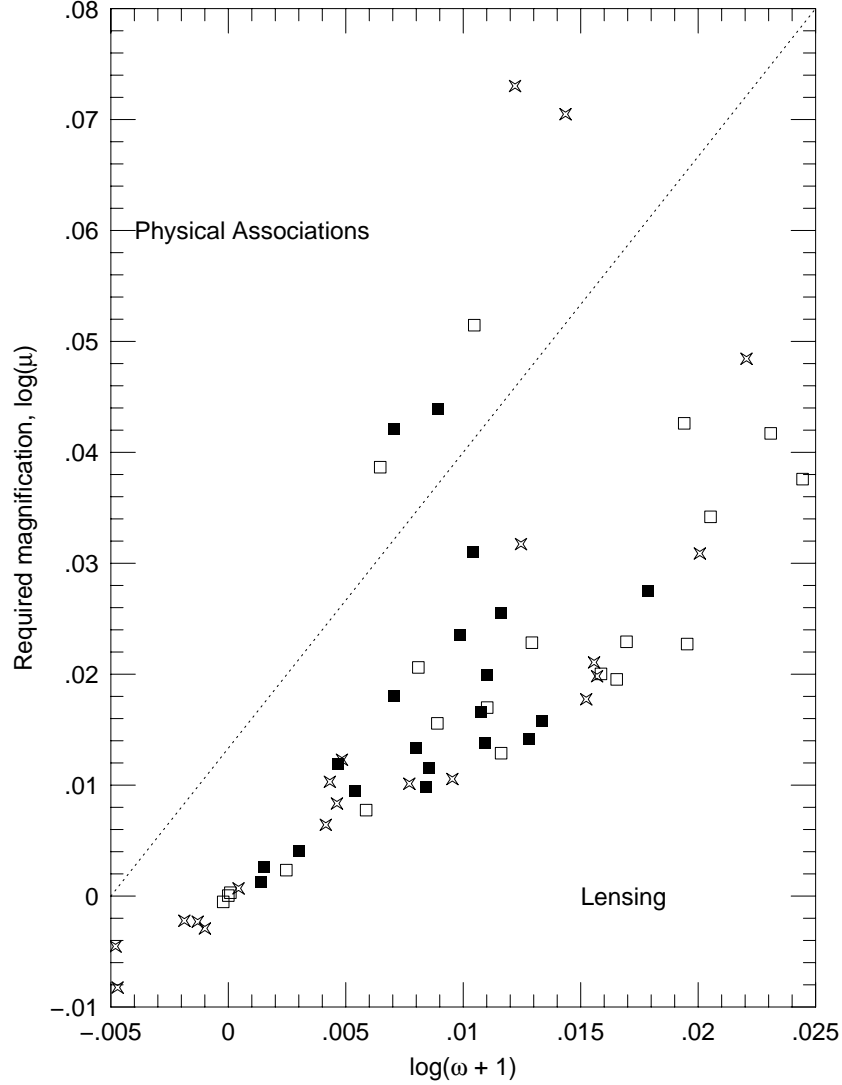


Fig. 9.— The required magnification to generate the measured integrated correlation, assuming lensing and given the measured slope of the QSO number-magnitude counts, $\alpha_m(z)$ for each redshift bin from Figure 4. X's, empty squares and filled squares correspond to points from $\omega(< 15')$, $\omega(< 30')$ and $\omega(< 60')$, respectively. The points can be separated between the two lowest redshift bins, and the rest. (The dotted line separating the two populations is, outside the fact that it divides the two populations, arbitrary.) The requirement to see such large magnifications to account for the measured correlations when compared to the rest of the points implies a different mechanism is the cause of the measured correlations: Physical associations.